Enhancing the Activity of Insulin at the Receptor Interface: Crystal Structure and Photo-Cross-Linking of A8 Analogues†

Zhuli Wan,[‡,§] Bin Xu,[‡,§] Kun Huang,[‡] Ying-Chi Chu,[||] Biaoru Li,[‡] Satoe H. Nakagawa,[⊥] Yan Qu,[‡] Shi-Quan Hu,[||] Panayotis G. Katsoyannis,[||] and Michael A. Weiss*[,‡]

Department of Biochemistry, Case Western Reserve University School of Medicine, Cleveland, Ohio 44106-4935, Department of Pharmacology and Biological Chemistry, Mt. Sinai School of Medicine of New York University, New York, New York 10029, and Department of Biochemistry and Molecular Biology, The University of Chicago, Chicago, Illinois 60637

Received August 17, 2004

ABSTRACT: The receptor-binding surface of insulin is broadly conserved, reflecting its evolutionary optimization. Neighboring positions nevertheless offer an opportunity to enhance activity, through either transmitted structural changes or introduction of novel contacts. Nonconserved residue A8 is of particular interest as $Thr^{A8} \rightarrow His$ substitution (a species variant in birds and fish) augments the potency of human insulin. Diverse A8 substitutions are well tolerated, suggesting that the hormone−receptor interface is not tightly packed at this site. To resolve whether enhanced activity is directly or indirectly mediated by the variant A8 side chain, we have determined the crystal structure of His^{A8}-insulin and investigated the photo-cross-linking properties of an A8 analogue containing *p*-azidophenylalanine. The structure, characterized as a $T_3R_3^f$ zinc hexamer at 1.8 Å resolution, is essentially identical to that of native insulin. The photoactivatable analogue exhibits efficient cross-linking to the insulin receptor. The site of cross-linking lies within a 14 kDa C-terminal domain of the α-subunit. This contact, to our knowledge the first to be demonstrated from the A chain, is inconsistent with a recent model of the hormone−receptor complex derived from electron microscopy. Optimizing the binding interaction of a nonconserved side chain on the surface of insulin may thus enhance its activity.

Insulin is a small protein that functions in the hormonal control of metabolism. After proteolytic processing of a single-chain precursor (proinsulin), the hormone consists of two chains, designated A (21 residues) and B (30 residues), and is stored in the pancreatic *β*-cell as a Zn-stabilized hexamer (*1*). Insulin functions in the blood as a monomer containing three α-helices and two extended segments (Figure 1A) (*2*−*4*). Because of its importance in the treatment of diabetes mellitus, insulin has attracted attention as a target of protein engineering (*5*). In recent years analogues have gained widespread clinical acceptance (*6*). Despite such empirical success, how insulin binds to the insulin receptor (IR)[1] is not well-understood. The IR comprises two extracellular α-subunits and two transmembrane *β*-subunits (Figure 1B; for review, see ref *7*). Binding of insulin to the α subunits activates the tyrosine kinase activity of the cytoplasmic domains of *β*-subunits, which leads in turn to a cascade of signal transduction events. Photo-cross-linking studies have demonstrated contacts between the α-subunit of the receptor and sites in the B chain (*7*−*10*). Our study defines a novel site of photo-cross-linking in the A chain and demonstrates how this site may be utilized to enhance the potency of insulin. The site of contact in the IR is inconsistent with a high-resolution model of the hormone−receptor complex (*11*) proposed on the basis of electron microscopic (EM) image reconstruction at a resolution of 20 Å (*12*, *13*).

The classical receptor-binding surface of insulin is conserved among vertebrate insulins, presumably reflecting its evolutionary optimization (*2*, *14*). Attention has thus focused on mechanisms by which substitutions at nonconserved sites may influence the biological and pharmacological properties of the hormone (*15*). Of particular interest is a substitution on the surface of the A chain, $Thr^{A8} \rightarrow His$ (arrow in Figure 1A; *16*, *17*). Originally observed in turkey insulin and

† This work was supported in part by the Diabetes Research and Training Center at the University of Chicago (S.H.N.) and grants from the National Institutes of Health to P.G.K. (DK56673) and M.A.W. (DK40949).

* To whom correspondence should be addressed. E-mail: michael.weiss@case.edu. Telephone: (216) 368-5991. Fax: (216) 368-3419.

‡ Case Western Reserve University School of Medicine.

§ These authors contributed equally to this work.

|| Mt. Sinai School of Medicine of New York University.

⊥ The University of Chicago.

[1] Abbreviations: [4E+A8H]insulin, analogue containing five substitutions ($Phe^{B1} \rightarrow Glu$, $His^{B10} \rightarrow Glu$, $Tyr^{B16} \rightarrow Glu$, $Thr^{B27} \rightarrow Glu$, and $Thr^{A8} \rightarrow His$) and lacking C-terminal residue Thr^{B30}; CD, circular dichroism; CR, cysteine-rich domain of the receptor α-subunit; Dab, diaminobutyric acid; DTT, dithiothreitol; EM, electron microscopy; Fn0−Fn2, fibronectin homology domains 1−3 of the receptor α-subunit, respectively; IGF-I, insulin-like growth factor I; IR, insulin receptor; IRα-N, polyclonal antiserum to the N-terminal epitope of the receptor α-subunit; L1 and L2, large domains 1 and 2 of the receptor α-subunit, respectively; NAv, NeutrAvidin; NMR, nuclear magnetic resonance; Pap, *p*-azido-Phe; Pmp, *p*-amino-Phe; rmsd, root-mean-square deviation; t_A or t_B tag, biotinylamido-caproyl modification of the N-terminus of the A or B chain, respectively; UV, ultraviolet; WGA, wheat germ agglutinin. Amino acids are designated by standard three- and one-letter codes.

10.1021/bi048223f CCC: $27.50
Published on Web 11/25/2004

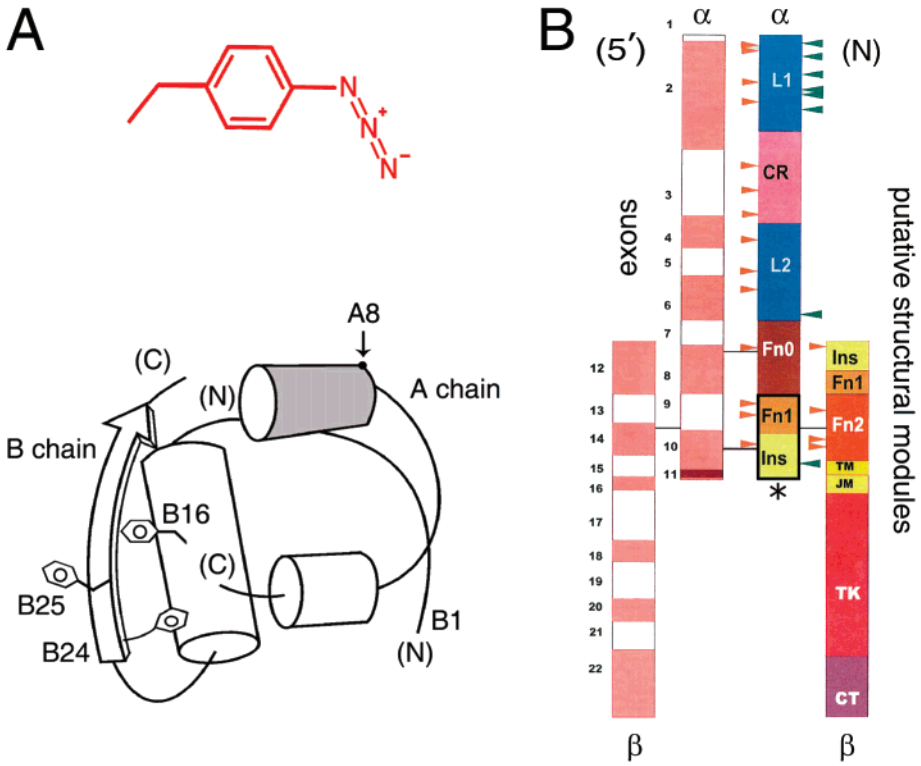

FIGURE 1: Structure of insulin and the insulin receptor. (A) Cylinder model of the insulin T-state protomer and structure of Pap (insert at top). The arrow represents residue A8, the C-cap of the A1−A8 A chain α-helix. Positions of other side chains discussed in the text (B16, B24, and B25) are as indicated. The proposed recognition helix is highlighted in gray. (B) Domain structure of the IR (right) and corresponding organization of exons in the IR gene (left). The α- and *β*-subunits are labeled. Putative structural models in the α-subunit (L1, CR, L2, Fn0, and the N-terminal portion of Fn1-ID) are inferred from homology modeling (*27*). Orange arrowheads indicate sites of N-linked glycosylation; green arrowheads indicate hot spots for mutations that impair binding of insulin. Numbers at the left designate exons.

characteristic of fish (red letters in Figure 2; *18*−*21*), His^{A8} enhances the thermodynamic stability of insulin (*17*) and augments its affinity for the insulin receptor by 2−5-fold with a commensurate increase in lipogenic potency (*17*, *22*−*24*). Whereas a general relationship between stability and biological activity has previously been proposed (*17*), studies of multiple A8 analogues indicate that effects on stability and activity are uncorrelated (*22*, *25*). Amino acids of diverse shape, size, and polarity are functionally well-tolerated (*25*), suggesting that this site is either not near the receptor or not tightly constrained at the receptor interface.

How does His^{A8} enhance the biological activity of insulin? This study addresses whether the variant A8 side chain indirectly modulates the structure of the conserved receptor-binding surface or instead introduces a novel receptor contact. Our approach has two parts. The crystal structure of His^{A8}-insulin is first determined to visualize the conserved receptor-binding surface. The structure, characterized by molecular replacement at 1.80 Å resolution, demonstrates that substitution of Thr^{A8} with histidine is readily accommodated in a native-like $T_3R_3^f$ hexamer[2] (*26*). The substitution does not significantly affect the conformations of the T or R protomers, their zinc-mediated assembly, or the ligand-induced T → R transition.[3] To investigate the role of the A8 side chain in the hormone−receptor complex, we next prepared a photoactivatable analogue containing *p*-azidophenylalanine (Pap, inset in red in Figure 1A) at this position. Packing of Pap^{A8} near the receptor is shown by its efficient cross-linking to the ectodomain. Surprisingly, proteolytic mapping of the covalent holoreceptor complex indicates that the site of cross-linking lies within a C-terminal 14 kDa fragment of the α-subunit. This fragment is derived from the fibronectin III homology domain (FnI) and the insert domain (ID, asterisk and black box in Figure 1B; *27*). These results are not in accord with a structural model derived from EM image reconstruction in which the A8 side chain is predicted to contact the N-terminal L1 *β*-helix (*11*). To our knowledge, this is the first explicit demonstration that the surface of the A chain contacts the insulin receptor as long envisaged (*2*, *28*, *29*). We propose that the ectodomain engulfs the insulin molecule to contact both its chains: His^{A8} augments activity by enhancing a nonconserved interaction at a novel edge of the hormone−receptor interface.

EXPERIMENTAL PROCEDURES

Design of Insulin Analogues. Six analogues of human insulin (Table 1) were prepared by chain combination: His^{A8}-

[2] The classical crystal forms of insulin contain zinc ions and are hexameric (T_6, $T_3R_3^f$, and R_6; *26*, *52*, *86*, *87*). The structure of an isolated T_2 dimer has also been determined in a Zn-free cubic lattice (*88*).

[3] The crystallographic TR transition, an allosteric reorganization of insulin hexamers (*52*, *87*), is remarkable for a change in the secondary structure of the B1−B8 segment from the extended (T state) to α-helix portion (R state). Segmental reorganization is coupled to changes in the conformation of Gly^{B8}, core packing, and handedness of cystine A7−B7. The latter sulfur atoms are exposed in the T state but buried in a nonpolar crevice in the R state. The superscript R^f refers to N-terminal fraying of the B1−B19 α-helix (*26*). The T → R transition has been analyzed as a model for the long-range transmission of conformational change (*89*).

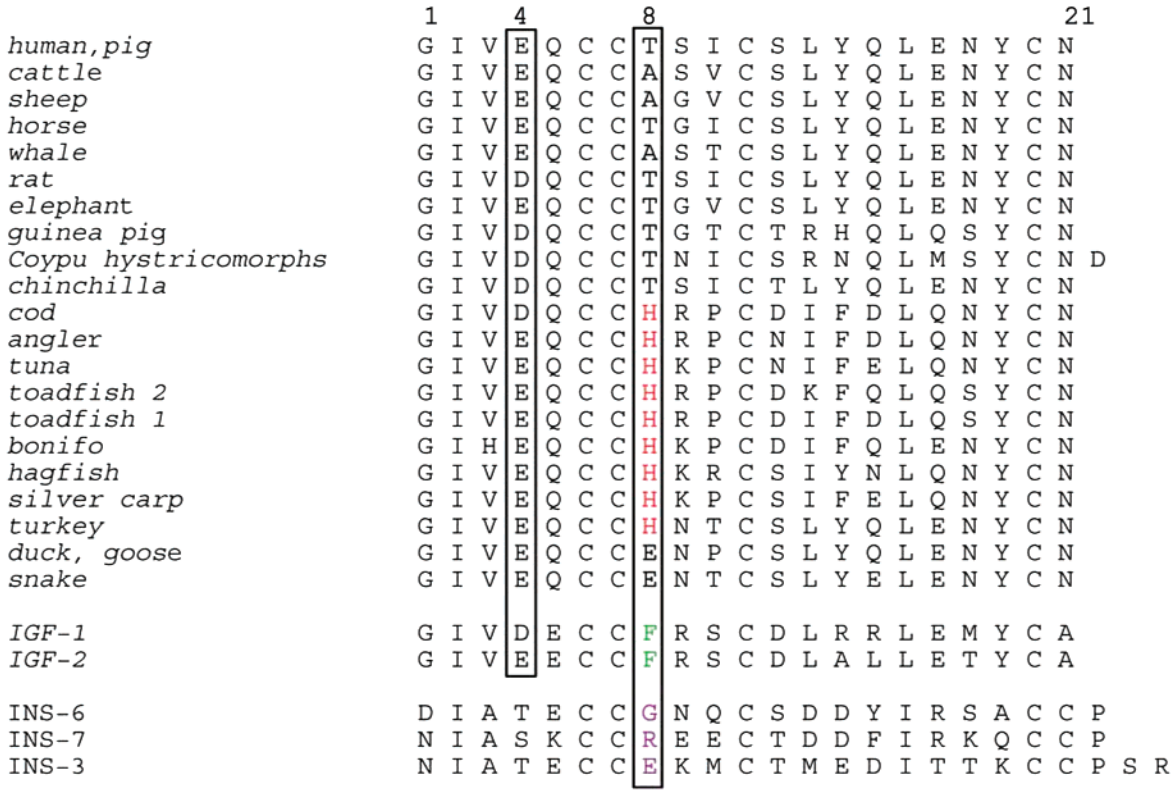

FIGURE 2: Sequences of insulin A chains in relation to the A domain of IGFs and representative β-class INS proteins of *Caenorhabditis elegans* (*85*). Residues A4 and A8 are boxed in black. Histidines at position A8 are colored red; corresponding residues in IGF and INS sequences are colored green and purple, respectively. Sequences were obtained from GenBank.

Table 1: Relative Receptor Binding Affinities of Insulin Analogues[a]

analogue	activity	analogue	activity
human insulin	100	His^{A8}-insulin[b]	212 ± 34 (4)
DKP-insulin[b]	161 ± 19 (4)	Pmp^{B0}-t_B-DKP-insulin	100 ± 14 (3)
t_B-DKP-insulin	132 ± 5 (3)	Pmp^{B16}-t_B-DKP-insulin	84 ± 8 (3)
Pmp^{A8}-t_B-DKP-insulin	238 ± 5 (3)	Pmp^{B25}-t_B-DKP-insulin	147 ± 3 (3)
Pmp^{A8}-t_A-porcine insulin[d]	52 ± 6 (3)	Glu^{A8}-DKP-insulin	61 ± 2 (3)[b]

[a] Values are relative to that of human insulin, which is assumed to be 100%. The number in parentheses indicates the number of repetitions. Pmp analogues each contain a biotin tag attached to the α-amino group of B1 (designated t_B) or the ϵ-amino group of D-lysine substituted at the A1 position (t_A). [b] Value obtained from Weiss et al. (*22*). The placental membrane assay at 4 °C underestimates the activity of high-potency analogues relative to cell-based binding studies and lipogenesis assays at higher temperatures (*22, 25*).

insulin for structural analysis and five Pap derivatives (positions A8, B0, B16, and B25; residue B0 refers to the N-terminal extension of the B chain by one residue). To facilitate characterization of photoproducts, four Pap derivatives were modified with a biotinylamido-caproyl tag at the N-terminus of the B chain as described previously (*10*). Because reduction of the disulfide bridges in Pmp^{A8}-t_B-DKP-insulin leads to separation of the biotin tag from the photoreactive probe (and hence following reduction of possible photo-cross-linked receptor domains on UV irradiation), an additional Pap^{A8} analogue was prepared in which the ϵ-amino group of D-Lys^{A1} (i.e., substituted for the native glycine at position A1) was likewise tagged with biotin. These respective tags are designated t_B and t_A in Table 1. His^{A8}-insulin was prepared using the native human B chain, whereas the DKP B chain was employed in syntheses of four Pap derivatives; "DKP" indicates substitutions that hinder formation of dimers (Pro^{B28} → Lys and Lys^{B29} → Pro) and hexamers (His^{B10} → Asp) (*4*, *30*−*33*). For synthetic convenience, the t_A-Pap^{A8} analogue was prepared using a porcine B chain, obtained from porcine insulin (a gift from Y. M. Feng, Institute of Biochemistry and Cell Biology, Chinese Academy of Sciences, Shanghai, China) by sulfitolysis. The human B chain *S*-sulfonate was likewise obtained from recombinant human insulin, generously provided by Eli Lilly and Co. (Indianapolis, IN).

Synthesis of Insulin Analogues. The general protocol for solid-phase synthesis of variant insulin chains is as described previously (*34*). In brief, 4-methylbenzhydrylamine resin (0.6 mmol of amine/g; Bachem, Inc.) was used as solid support for synthesis of A chain analogues; (*N-tert*-butoxycarbonyl,*O*-benzyl)threonine-PAM resin (0.56 mmol/g; Bachem, Inc.) was used as a solid support for synthesis of B chain analogues. A manual double-coupling protocol was followed (*35*, *36*). Protection of the *p*-NH_2 moiety of Phe (designated Pmp) was carried out by the 2-chlorobenzyloxycarbonyl group, which is stable under the conditions employed in the stepwise synthesis of A and B chain analogues. Chain recombination employed S-sulfonated A and variant B chains (approximately 2:1 by weight) in 0.1 M glycine buffer (pH 10.6) in the presence of dithiothreitol (*35*). Insulin analogues were isolated from the combination mixture (*36*) and purified as described previously (*22*); essentially native yields were obtained. Mass spectrometry in each case gave expected values. Conversion of *p*-amino-Phe to Pap in the intact hormones (*10*) was verified by mass spectrometry. Purity was in each case greater than 98% as evaluated by analytical reverse-phase HPLC. Electrospray mass spectra revealed no anomalous molecular masses.

X-ray Crystallography. Crystals were grown by hanging-drop vapor diffusion in the presence of a 1:2.5 Zn^{2+}:protein monomer ratio and a 3.7:1 phenol:protein monomer ratio in Tris-HCl buffer as described previously (*37*). Drops consisted of 2 μL of protein solution (10 mg/mL in 0.02 M HCl) mixed with 2 μL of reservoir solution [0.02 M Tris-HCl, 0.05 M sodium citrate, 5% acetone, 0.03% phenol, and 0.01% zinc acetate (pH 8.4)]. Each drop was suspended over 1 mL of reservoir solution. A cosolvent (either acetone, phenol, or glycerol) was found to be essential for crystallization; in its absence, the protein forms an amorphous precipitate. Crystals (space group *R*3) were obtained at room temperature after 2 weeks. Data were collected from single crystals mounted in a rayon loop and flash-frozen to 100 K. Reflections from 19.2 to 1.8 Å were measured with a CCD detector system using synchrotron radiation at the Advanced Photon Source (beam line 14BMD, Argonne National Laboratories, Argonne, IL). Data were processed with DENZO (version 1.9.6) and SCALEPACK (version 1.9.6). The crystal belongs to space group R_3 with the following unit cell parameters: $a = b = 79.34$ Å, $c = 34.71$ Å, $\alpha = 90°$, $\beta = 90°$, and $\gamma = 120°$. The structure was determined by molecular replacement using CNS (*38*). Accordingly, a model was obtained using the native TR dimer [Protein Data Bank (PDB) entry 1TRZ following removal of all water molecules, zinc ions, and chloride ions]. A translation-function search was performed using coordinates from the best solution for the rotation function following analysis of data between 15.0 and 4.0 Å resolution. Rigid-body refinement using CNS, employing overall anisotropic temperature factors and bulk-solvent correction, yielded values of 0.315 and 0.336 for *R* and R_{free}, respectively, for data between 19.2 and 3.0 Å resolution. Between refinement cycles, $2F_o - F_c$ and $F_o - F_c$ maps were calculated using data to 3.0 Å resolution; a phenol molecule was built into the TR^f structure using *O* (*39*). The geometry was continually monitored with *PROCHECK* (*40*); zinc ions and water molecules were built into the difference map as the refinement proceeded. Calculation of omit maps and further refinement were carried out using CNS (*38*) and X-PLOR (*41*), which implement maximum-likelihood torsion-angle dynamics and conjugate-gradient refinement. Statistics are provided in Table 2.

Table 2: X-ray Diffraction and Refinement Statistics

resolution limit (Å)	19.18−1.8
R	0.189
R_{free}	0.245
R_{mere}	
all data	0.048
overall	23.52
highest-resolution shell	0.224
$I/\sigma(I)$	9.2
overall	
no. of reflections used	7426
completeness (%)	98.4
redundancy	4.3
no. of protein atoms	823
no. of water molecules	138
highest-resolution shell	
resolution range (Å)	1.91−1.80
no. of reflections	1075
completeness (%)	95.4
redundancy	2.8
R	0.202
R_{free}	0.238
rmsd from standard geometry	
bond lengths (Å)	0.006
bond angles (deg)	1.2
dihedral angles (deg)	20.3
improper angles (deg)	0.64
cross validation from estimated error	
ESD from *C*−*V* Luzzati plot	0.25
ESD from *C*−*V* sigma	0.02
Ramachandran plot	
residues in the most favored region (%)	91.9
residues in the additional allowed region (%)	8.1
isotropic thermal model restraints (Å^2)	
main chain bonds	1.45
main chain angles	2.30
side chain bonds	2.12
side chain angles	3.13
average *B* factor	28.83
protein	28.61
solvent	31.62

Lectin Purification of the Insulin Receptor. The human insulin receptor (IR) was partially purified from Chinese hamster ovary (CHO) cells stably transfected to overexpress the B-splicing isoform of the human receptor (P3-A; kindly provided by D. F. Steiner) (*42*). Methods of cell culture and wheat germ agglutinin (WGA) purification were as described previously (*42*). Cells were detached using Hank's-based enzyme-free cell dissociation buffer (Invitrogen Life Technologies). Specific binding of insulin to the WGA-purified IR was verified with polyethylene glycol 8000 precipitation according to the method of Schäffer (*43*). The recombinant ectodomain of the IR, purified from a bacculoviral expression system (*44*), was kindly provided by G. D. Smith and C. Yip (University of Toronto, Toronto, ON).

Receptor Binding Assays. Receptor binding assays (Table 1) were performed using a human placental membrane (*45*) as described previously (*22*). Relative activity is defined as the ratio of analogue to human insulin required to displace 50% of specifically bound human [^{125}I]insulin (Amersham). In all assays, the percentage of tracer bound in the absence of the competing ligand was less than 15% to prevent ligand-depletion artifacts. Each determination was performed with three or four replicates; values are reported as the mean and standard deviation (Table 1). This assay underestimates activities for analogues whose affinities are more than 2-fold higher than that of native insulin (*22*).

Photo-Cross-Linking Studies. A protocol for photo-cross-linking studies has recently been described (*46*). In brief, the soluble ectodomain or WGA-purified IR was mixed in the dark with photoactive insulins labeled at indicated positions at a concentration of 200 nM at 4 °C with gentle shaking overnight. Binding solutions were then transferred to a Costar assay plate (Corning Inc.) for ultraviolet (UV) irradiation. Short-wave UV radiation (254 nm) generated from a Mineralight Lamp (model UVG-54, UVP, Upland, CA) was used with an optimum exposure time of 20 s and a distance from the light source of 1 cm. After cross-linking, the hormone−receptor complex was reduced with dithiothreitol (DTT) and resolved by 10 to 20% gradient SDS−PAGE. The separated proteins were then blotted onto a nitrocellulose membrane. Cross-linked adducts were probed with NeutrAvidin (NAv; Pierce). To verify the identity of the α-subunit of the insulin receptor, gels were also probed with anti-IRα antiserum (IR_α-N; Santa Cruz Biotechnology, Santa Cruz, CA), which recognizes the N-terminal 20-amino acid sequence of the α-subunit (i.e., the L1 domain). Sites of cross-linking in the IR were mapped by partial proteolysis

to discrete regions of the α-subunit. This strategy utilizes the Pap^{B25} derivative to provide a fingerprint of binding to the C-terminal domain of the α-subunit (*10*) and the Pap^{B16} derivative as a probe of the N-terminal L1 domain (*47*). Partial proteolysis takes advantage of previous characterization of chymotryptic sites as described (*48*, *49*), in particular, a protected 47 kDa N-terminal glycosylated fragment containing the L1 β-helix and part of the CR domain (see below).

Chymotryptic Digestion. WGA-purified receptors were cross-linked with photoactive insulins and digested at 37 °C with 100 μg/mL chymotrypsin (Sigma, St. Louis, MO) in a solution of 50 mM HEPES (pH 7.4) containing 0.1% Triton X-100 and 0.11 M NaCl. Digestions were stopped at successive times by heating aliquots at 95 °C for 5 min. An equal volume of Laemmli sample buffer was added, and the mixtures were treated (or not treated) with 100 mM DTT. Digestion mixtures were analyzed by 12.5% SDS−PAGE, blotting onto nitrocellulose membrane, and probed with NeutrAvidin or an anti-IRα antiserum (N-20) as described above. Proteolytic mapping also permitted specific cross-linking efficiencies to be estimated on the basis of the observation of an SDS−PAGE mobility shift between native proteolytic fragments of the α-subunit and their corresponding A or B chain adducts. Except for the low-efficiency Pap^{B0} derivative, the ratio of shifted to unshifted bands was 20−30%, indicating that the efficiency of photo-cross-linking is at least this high. Efficiencies might be higher if the WGA-purified IR was not completely active, since inactive receptors would only contribute to the unshifted bands.

Deglycosylation of the Insulin Receptor and Chymotryptic Fragments. Chymotryptic fragments of the Pap-cross-linked IR complexes were deglycosylated with peptide-N-Glycosidase F (N-Glycanase; Prozyme). Samples were denatured at 95 °C for 5 min in 20 mM sodium phosphate (pH 7.5) containing 0.1% SDS and 50 mM β-mercaptoethanol prior to deglycosylation. The solutions were cooled to room temperature, and nonionic detergent NP-40 (final concentration of 0.75%) and N-Glycanase (1 milliunit per microgram of receptor in the initial chymotryptic digestion) were added. Samples were incubated at 37 °C for 4 h. The reaction was stopped by heating at 95 °C for 10 min. An equal volume of Laemmli sample buffer was added for SDS−PAGE. Control deglycosylation of the intact α-subunit indicated complete conversion of the 135 kDa glycoprotein band to a 98 kDa band in accord with past studies (*50*).

Interpretation of Molecular Masses. A Pap^{B16} insulin derivative has previously been shown to cross-link within the L1 domain (residues 1−158; *47*). The electrophoretic mobility of the B16-cross-linked N-terminally glycosylated chymotryptic fragment corresponds to a molecular mass of 50 kDa; following enzymatic deglycosylation, the apparent mass is 31 kDa (including the B chain adduct). These masses suggest a fragment of ca. 250 residues containing four or five glycosylation sites (orange arrowheads in Figure 1B). The putative structure (as obtained by homology modeling; *27*) predicts prominent chymotryptic sites between residues 245 and 260 in the cysteine-rich (CR) domain (YYHFQDWRCVNFSFCQ sequence), exposed on the back surface of the domain (*51*). Cleavage within this segment would yield (in the absence of glycosylation) 29−30 kDa fragments. C-Terminal chymotryptic fragments are identified on the basis of cross-linking to the Pap^{B25} insulin derivative, previously shown to contact a peptide spanning residues 704−718 (*10*). Pap^{B25}-cross-linked chymotryptic fragments thus provide a fingerprint for cross-linking to the C-terminal tail of the α-subunit. B25-cross-linked chymotryptic fragments exhibit apparent masses of 34 and 20 kDa when glycosylated; on deglycosylation, these fragments run as 23 and 17 kDa bands, respectively (inclusive of the B chain adduct). The latter receptor fragment contains ca. 110−130 amino acids and so provides a probe for the Fn1/ID region (asterisk in Figure 1B). This chymotryptic fragment is slightly smaller than the canonical homology region (residues 590−731; 142 amino acids). The mass difference on deglycosylation (3 kDa) indicates that the fragment contains at least one N-linked carbohydrate; the Fn1/ID region contains three N-linked sites of glycosylation (residues 605, 624, and 671; Figure 1B).

RESULTS

Our study has two parts. The crystal structure of His^{A8}-insulin is first determined in an effort to investigate whether transmitted changes occur in the conformation of the classical receptor-binding surface. Photo-cross-linking studies of Pap^{A8} are then described to test whether and where the A8 side chain contacts the IR. Pap substitutions at three sites in the B chain are employed as controls. The photoactivatable side chain was introduced into an engineered insulin monomer (DKP-insulin), chosen as a template for its efficiency of synthesis, its enhanced receptor binding, and the absence of confounding self-association (*4*). Biotin tags were introduced during synthesis to facilitate detection of photo-cross-linked domains of the insulin receptor. Structural details of the His^{A8} hexamer and statistical analyses are described in the Supporting Information.

Structural Studies. His^{A8}-human insulin was crystallized as a $T_3R_3^f$ zinc hexamer[4] in a lattice similar to that of rhombohedral four-Zn insulin (*52*). The lattice contains a TR^f dimer in the asymmetric unit; the hexamer is generated by crystallographic symmetry. The structure was determined by molecular replacement. The refined model (determined to a resolution of 1.80 Å at 100 K) includes all residues in each chain and 138 water molecules. Its *R* factor equals 0.189, and R_{free} equals 0.245; diffraction parameters, data collection statistics, and additional *R* factors are given in Table 2.

The overall structure is similar to that of native insulin (Figure 3). The organization of the hexamer is essentially identical to that of native insulin in the same crystal form. No significant changes are observed in secondary structure, chain orientation, mode of assembly, or structure of Zn^{2+}-binding sites (Figure 4). The two Zn^{2+}-binding sites are each well-defined without evidence of multiple ligand conformations (see the Supporting Information). As expected, in the T_3 trimer, Zn^{2+} coordination geometry is octahedral. Ligation is mediated by three symmetry-related His^{B10} side chains with Zn−N distances of 2.02 Å; the remaining coordination sites are occupied by symmetry-related water molecules with Zn−O distances of 2.43 Å and a chloride ion with a Zn−Cl

[4] The dimensions of this unit cell ($a = b = 79.34$ Å, $c = 34.71$ Å, $\alpha = \beta = 90°$, and $\gamma = 120°$) are characteristic of a $T_3R_3^f$ hexamer (*26*).

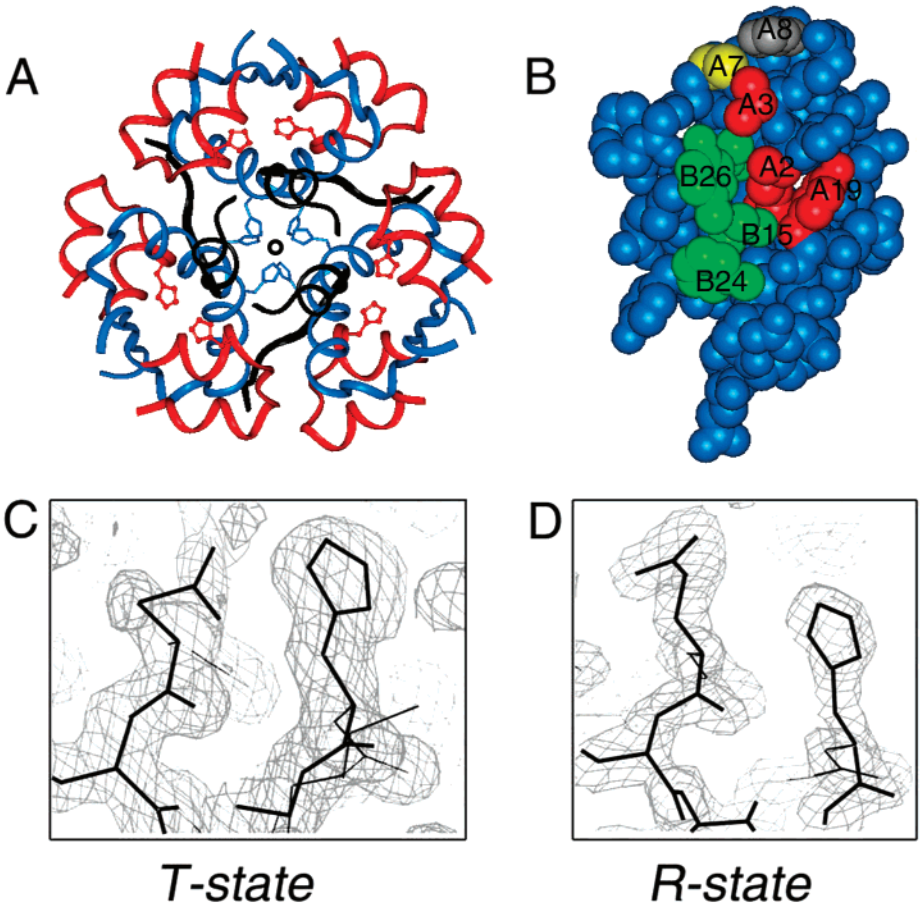

FIGURE 3: Crystal structure of human His^{A8}-insulin. (A) Overview of the variant $T_3R_3^f$ zinc hexamer. The A chain is shown in red, the B1−B8 segment in black, and the remaining B chain in blue. The side chains of His^{A8} (red) and His^{B10} in the Zn^{2+} coordination site (blue) are shown. (B) Space-filling representation of the T-state protomer showing His^{A8} in relation to the classical receptor-binding surface. (C and D) The $2F_o - F_c$ electron density maps of molecule 1 (C; T state) and molecule 2 (D; R state) showing atomic positions of residues of A1−A5 in His^{A8}-insulin. Maps are contoured at 1.0σ.

distance of 2.25 Å. In the R_3^f trimer, the coordination geometry is tetrahedral. Ligation is mediated by three symmetry-related His^{B10} side chains with Zn−N distances of 2.06 Å; the fourth site is occupied by a chloride ion with a Zn−Cl distance 2.26 Å. The phenol-binding sites in the R_3^f trimer are similar to those previously described[5] (Supporting Information; *26*, *53*). Root-mean-square deviations (rmsds) between respective main chain atoms in variant and native structures[6] are 0.56 Å (T state) and 0.58 Å (R state); respective side chain rmsd values (excluding A8) are 1.32 and 1.21 Å. These values are similar to those obtained in pairwise comparison between structures of native insulin in different crystal forms (Supporting Information).

The classical receptor-binding surface and hydrophobic core of insulin (*2*, *28*) are unaffected by the A8 substitution. In particular, the conformation and environment of conserved residues Ile^{A2}, Val^{A3}, Leu^{A16}, Tyr^{A19}, Leu^{B6}, Leu^{B11}, Val^{B12}, Leu^{B15}, Tyr^{B16}, Phe^{B24}, Phe^{B25}, and Tyr^{B26} are similar to those of the native $T_3R_3^f$ zinc hexamer. The canonical disulfide bridges are likewise unperturbed. Local conformational adjustments are nonetheless apparent near the site of substitution. The T-state protomer of His^{A8}-insulin contains a salt bridge (distance of 2.84 Å) between the side chain carboxylate of Glu^{A4} and the imidazole of the variant A8 side chain ($O^{\epsilon 1}-N^{\delta}$); the native salt bridge between Glu^{A4} and the α-amino group of A1 is broken. The A4−A8 distance predicts formation of a charge-stabilized hydrogen bond (Figure 5A). The neighboring side chain of Gln^{A5} exhibits two conformations.[7] By contrast, the conformation of His^{A8} in the R-state protomer is similar to that of Thr^{A8} in the native R state. In each case, no interactions are observed between A4 and A8 side chains (Figure 5B). The distance between the side chain carboxylate of Glu^{A4} and the imidazole of the variant A8 side chain ($O^{\epsilon 1}-N^{\delta}$) is 7.25 Å. The environment of His^{A8} in the T and R state resembles those of the homologous aromatic side chain (Phe^{A8}) in the crystal

[5] The orientation of phenol is stabilized in part by hydrogen bonds from the phenolic hydroxyl group to the carboxyl oxygen of Cys^{A6} (O···O distance, 2.43 and 2.66 Å; Protein Data Bank entries 1MPJ and 1LPH, respectively) and the nitrogen of Cys^{A11} (O···N distance, 2.91 and 3.20 Å; Protein Data Bank entries 1MPJ and 1LPH, respectively); see the Supporting Information for a view of this site.

[6] An estimate of the intrinsic variability among wild-type insulin crystal forms is provided by mean pairwise rms deviations, defined as the average of rmsd values obtained in systematic pairwise alignment of main chain atoms. This measure provides a baseline for assessment of rms deviations between the variant and native structures.

[7] The two conformations of Gln^{A5} in the T state are equally populated and are characterized as follows. In the first conformer, the side chain χ_1 and χ_2 dihedral angles are −89° and 50°, respectively. The diagnostic distance between the ϵ_1 oxygen atom of Gln^{A5} and the carboxyl oxygen atom of Gly^{A1} is 2.75 Å; the distance between the ϵ_2 oxygen atom of Gln^{A5} and the hydroxyl oxygen atom of Tyr^{A19} is 4.55 Å. In the second conformer, corresponding (χ_1 and χ_2) dihedral angles are −80° and −164° and diagnostic distances are 4.82 and 2.76 Å, respectively.

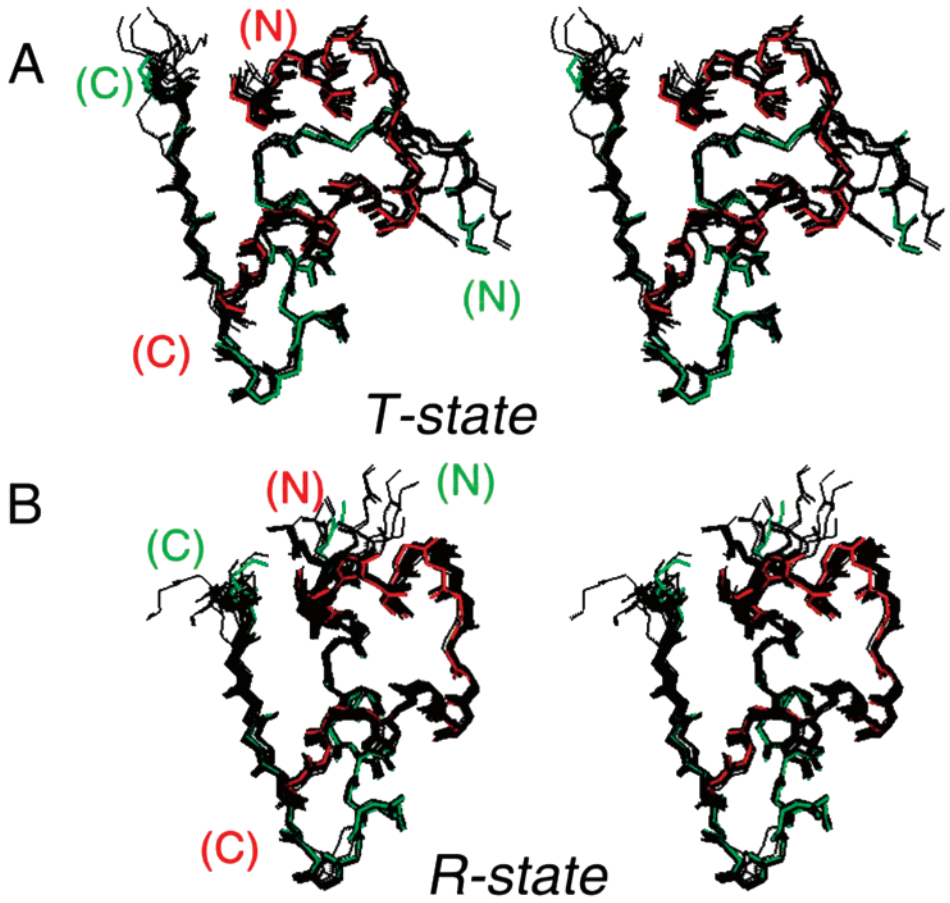

FIGURE 4: Stereopairs of T-state (A) and R-state (B) protomers showing the structure of the variant in relation to native insulin. The A and B chains of His^{A8}-insulin are colored red and green, respectively; native structures are colored black. Structures are aligned with respect to main chain atoms of residues A1−A21 and B3−B28 (T-state coordinates were obtained from PDB entries 4INS, 2INS, 6INS, 1APH, 1BPH, 1CPH, 1DPH, 1MPJ, 1TRZ, 1TYL, 1TYM, 1LPH, and 3MTH; R-state coordinates were obtained from PDB entries 1BEN, 1MPJ, 1TRZ, 1TYM, 1LPH, 3MTH, 1G7A, 1ZEG, 1ZEN, and 1ZNJ).

structure of IGF-I (Figure 5C). Because diverse A8 substitutions are likely to induce variations in stability or segmental helical structure without correlation with biological activities (*54*), such local variations are unlikely to be functionally significant.

The structure of insulin in solution resembles the crystallographic T state (*3*, *4*). The rmsd values of His^{A8}-insulin in relation to homonuclear NMR models of [4E+A8H]insulin (PDB entry 1IOH; *3*) are larger than deviations observed among native T- or R-state crystal structures. The His^{A8} analogue employed in NMR studies (designated [4E+A8H]-insulin) contained four substitutions in the B chain and lacked Thr^{B30} (*55*). Only a T-like secondary structure is observed in solution; no evidence was detected of an A4−A8 salt bridge. Although significant differences are observed relative to the crystal structure presented here (see Supporting Information), in each case an absence of transmitted structural perturbations is seen relative to respective parent structures. Mean rmsd values between respective main chain atoms are 1.81 Å (T state), whereas side chain rmsd values (excluding variant residues B1, B10, B16, B27, and B30) are 2.70 Å (Supporting Information). The range of conformations of the His^{A8} side chain in solution ($\chi_1 = -84.2 \pm 11.7°$ and $\chi_2 = -16.2 \pm 21.0°$; average and standard deviation among 26 NMR models) is similar but not identical to those presently observed in the crystallographic R-state protomer ($\chi_1 = -65°$ and $\chi_2 = -22°$). By contrast, the crystallographic T-state protomer exhibits a distinct value of χ_2 ($\chi_1 = -65°$ and $\chi_2 = 176°$) in association with the A4−A8 interaction. In accordance with an α-helical structure, the main chain (ϕ and ψ) dihedral angles of His^{A8} (−73.0° and −31.4°, respectively) in the T state and (−82.3° and −25.5°, respectively) in the R state are within the range of those observed in solution ($\phi = -84.2 \pm 11.7°$ and $\psi = -16.2 \pm 21.0°$). It is not known whether the imprecision of the NMR ensemble reflects true physical disorder or limitations of homonuclear NMR methods.

Photo-Cross-Linking Studies. To test whether residue A8 is near the IR, we synthesized an analogue containing Pap, a photoactivatable derivative of phenylalanine (*56*). Pap was chosen on the basis of its rigidity and small size (relative to other photoactivatable moieties), thus limiting the distance range for cross-linking. Pap was previously introduced at B25 by Kurose et al. and shown to cross-link near the C-terminus of the α-subunit of the insulin receptor[8] (*10*). A corresponding Pap^{B25} derivative was thus prepared to provide a fingerprint for photo-cross-linking to the C-terminal domain. Additional controls were prepared at position B16 in the classical receptor-binding surface (shown to contact

[8] Kurose et al. characterized a Pap^{B25} derivative of the truncated insulin analogue *des*[B26−B30]insulin-amide containing a B1 biotin tag. The Pap moiety was found to cross-link within the insert subdomain of the α-subunit (i.e., near the extreme C-terminus; *10*).

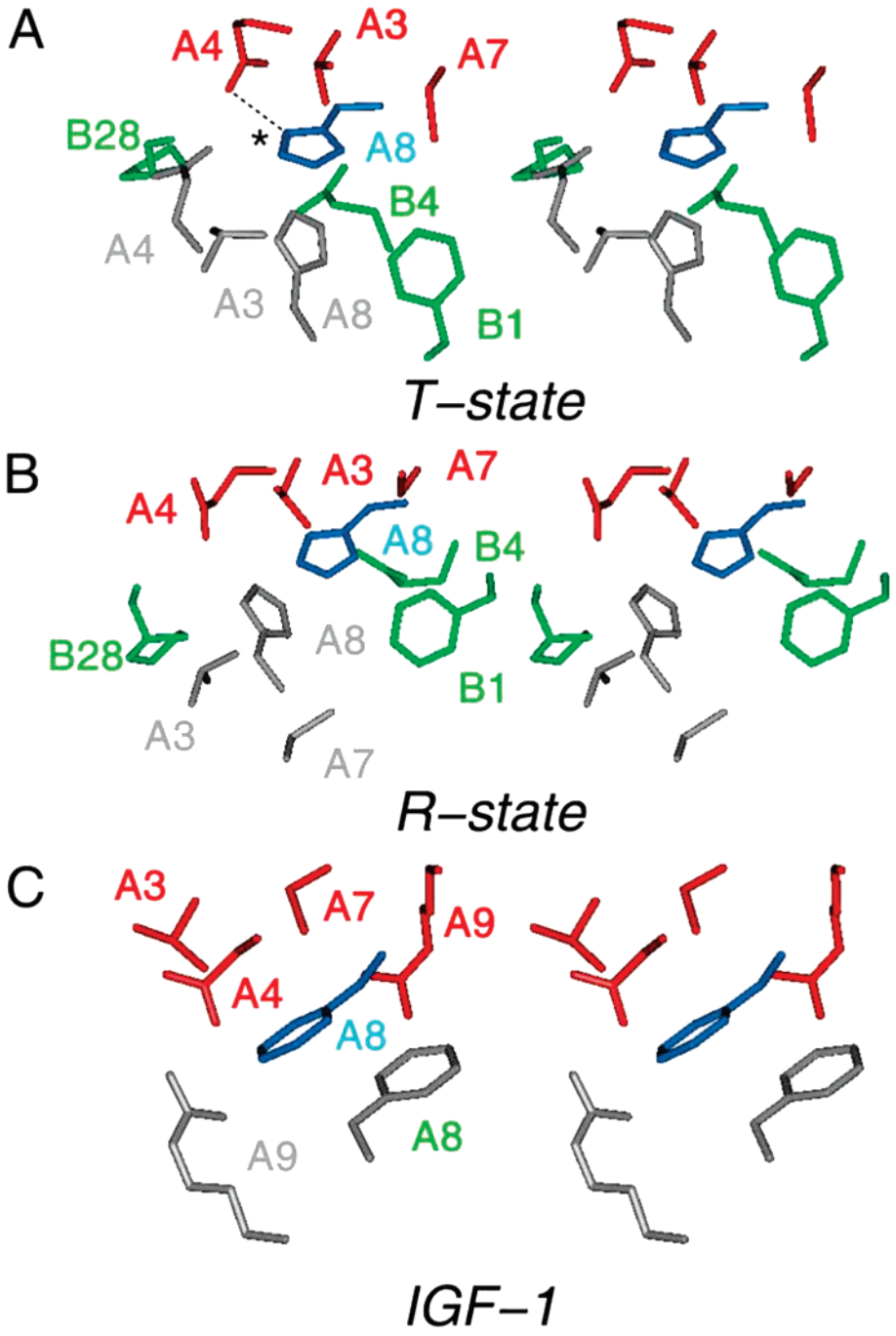

FIGURE 5: Packing schemes involving His^{A8}. (A) Environment of His^{A8} (blue; see the asterisk) in the T-state protomer in relation to selected A chain residues [Val^{A3}, Glu^{A4}, and Cys^{A7} (red)], B chain residues [Phe^{B1}, Gln^{B4}, and Pro^{B28} (green)], and trimer-related residues [Val^{A3}, Glu^{A4}, and His^{A8} (gray)]. In the T-state protomer, His^{A8}-insulin participates in a salt bridge to the side chain carboxylate of Glu^{A4} ($O^{\epsilon 1}-N^{\delta}$); the asterisk denotes a distance of 2.84 Å. (B) Corresponding environment of His^{A8} in the R state. The color scheme is the same as that in panel A. No A4−A8 salt bridge is observed. (C) Analogous environment in IGF-I (PDB entry 1IMX). Environment of Phe^{A8} [homologous to His^{A8} (blue)] in the crystal structure in relation to residues homologous to Val^{A3} (red), Glu^{A4} (red), Cys^{A7} (red), Ser^{A9} (red), and His^{A8} (green). Although IGF-I does not form a dimer or hexamer in the crystal, a symmetry-related residue (Ser^{A9}) provides a lattice contact (gray). Phe^{A8} is residue 49 of IGF-I; the numbering scheme in panel C differs from the standard IGF convention to highlight the relationship to insulin.

the N-terminal L1 domain; *47*) and as an amino-terminal extension of the B chain (Pap^{B0}). Because residues B1−B4 are dispensable for receptor binding (*2*), the latter was expected to cross-link only weakly.[9] Although the lability of the Pap moiety limits assessment of relative activities, the *p*-amino-Phe precursor is stable. The Pmp forms of these analogues in each case exhibit high affinity for the IR (Table 1). Interestingly, although the t_B-tagged derivative of DKP-insulin is less active than DKP-insulin, substitution of Thr^{A8} with Pmp increases its activity by ~2-fold. Thus, diverse aromatic side chains at A8 (Pmp, His, and Trp; *57*) are associated with increased receptor affinity. By contrast, Pmp

[9] A similar B0 photoactivatable derivative was previously prepared by Brandenberg and colleagues (*62*). Although this analogue was shown to cross-link to residues 390−488 of the α-subunit, the efficiency of cross-linking was not determined. We suggest that the long and flexible tether provided by residues B0−B4 enables nonspecific low-efficiency cross-linking to distant surfaces of the IR.

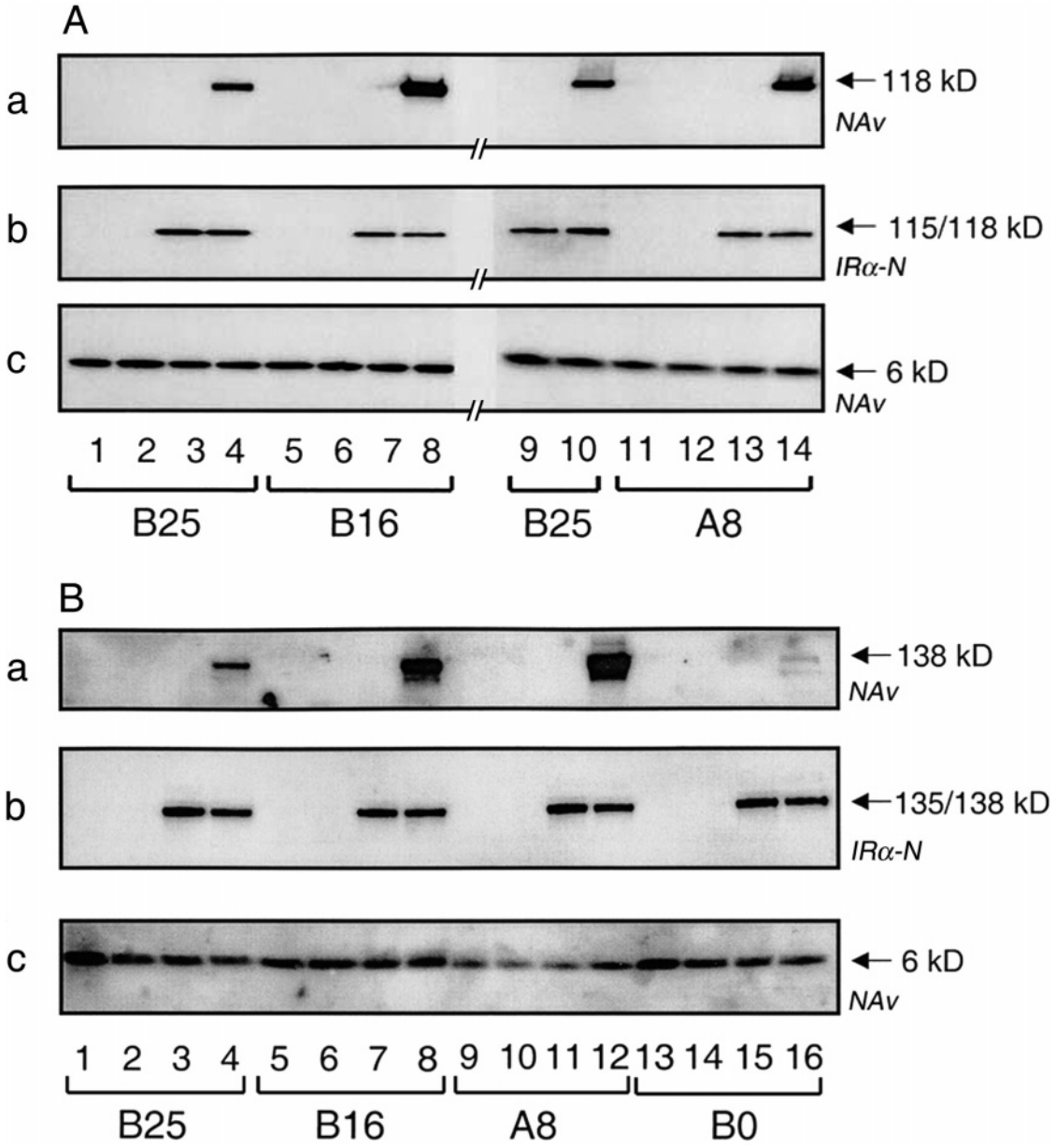

FIGURE 6: Photo-cross-linking of Pap^{A8}-DKP-insulin and control analogues to (A) the isolated ectodomain and (B) the lectin-purified holoreceptor. Analysis of photoproducts by SDS−PAGE and Western blotting using NeutrAvidin (NAv) to detect the biotin tag on the insulin B chain (boxes a and c in each panel) or polyclonal antiserum (IRα-N) to detect N-terminal residues of the α-subunit (box b). (A) Photo-cross-linking via positions B25 (lanes 4 and 10), B16 (lane 8), and A8 (lane 14) analyzed following DTT reduction. Lanes 1−3, 5−7, 9, and 11−13 show control reaction mixtures in which either the ectodomain had been omitted (lanes 1, 2, 5, 6, 11, and 12) or samples had not been irradiated (lanes 1, 3, 5, 7, 9, 11, and 13). (b and c) Control blots to demonstrate that equal amounts of ectodomain (b, with DTT) and insulin derivatives (c, without DTT) were present in each reaction. (B) Photo-cross-linking to WGA-purified IR: (a) photo-cross-linking via positions B25 (lane 4), B16 (lane 8), A8 (lane 12), and B0 (lane 16) analyzed following reduction by DTT. Lanes 1−3, 5−7, 9−11, and 13−15 show control reaction mixtures in which either the IR had been omitted (lanes 1, 2, 5, 6, 9, 10, 13, and 14) or samples had not been irradiated (lanes 1, 3, 5, 7, 9, 11, 13, and 15). Boxes b and c are control blots as in panel A. Molecular masses are in each case shown at the right.

substitution at B16 and the Pmp extension at B0 cause small decreases in the level of receptor binding. Because photo-cross-linking reactions are performed at high concentrations of the ligand and receptor (200 nM) relative to the native dissociation constant (ca. 0.2 nM), such changes in relative affinity do not affect efficiencies of cross-linking.

Following UV irradiation, A8, B16, and B25 Pap analogues each exhibit efficient cross-linking to the isolated ectodomain and WGA-purified IR (Figure 6). At least 20% of bound probes form covalent complexes as indicated by analysis of chymotryptic digestions (see below). Photo-cross-linking is successively weakened by addition of native insulin, or at higher ligand concentrations, IGF-I, indicating that the Pap derivatives are binding to the specific hormone-binding pocket. No competition is observed with unrelated proteins (hen egg white lysozyme or nonspecific immunoglobulins). Remarkably, cross-linking efficiency is greatest at A8. This does not imply that Pap^{A8} is closer to the receptor than residue B16 or B25 since the photochemistry of cross-linking can be influenced by local environment (*56*); the presence of hydrophilic functional groups near A8, for example, might be more highly reactive with the Pap probe than a putative nonpolar interface near B16 or B25 (*56*). In contrast to the efficiency of cross-linking at the sites

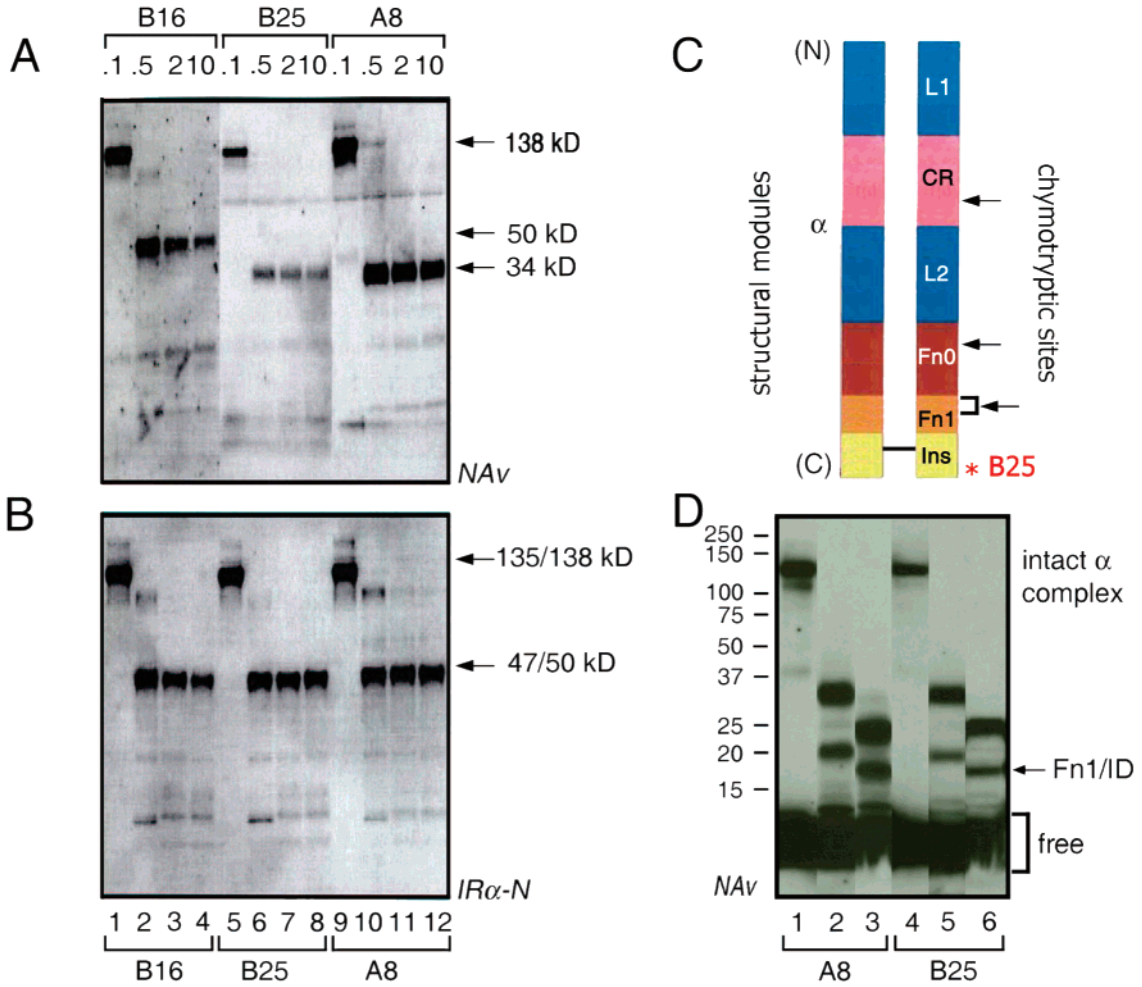

FIGURE 7: Mapping of hormone−receptor contacts by limited chymotryptic digestion. (A and B) Corresponding NAv-detected (A) and IR_{α}-N-detected (B) blots following the initial time course of digestion of B16-, B25-, and A8-cross-linked complexes. The time periods of digestion (0.1, 0.5, 2, and 10 min) are indicated at the top. The molecular mass of the intact α-subunit is 135 kDa (including glycosylation). Limited chymotryptic digestion liberates a 47 kDa N-terminal domain (50 kDa including the mass of the tethered B chain; lanes 1−4) and 34 kDa fragment (including the tethered B chain; lanes 5−8 in panel A) containing the C-terminal B25 contact site (704−718 peptide; *10*). The A8 digestion pattern (lanes 9−12 in panel A) mirrors that of the Pap^{B25}-cross-linked complex. B16 and B25 analogues contain a biotin tag at the α-amino group of B1; the A8 analogue contains a biotin tag at D-Lys^{A1} (see the footnote of Table 1). (C) Schematic outline of the α_2 dimer showing putative structural models (L1, CR, L2, Fn0, and the N-terminal portion of Fn1/ID) and sites of preferential chymotryptic cleavage of cross-linked hormone−receptor complexes (arrows). Additional central cleavage sites are possible but would not be probed by NAv−biotin adducts or IRα-N Western blotting. The red asterisk indicates the site of photo-cross-linking by $PapB^{25}$ (*10*). (D) Further chymotryptic digestions of A8- and B25-cross-linked complexes yield similar 20 kDa glycosylated C-terminal fragments (lanes 2 and 5; including the mass of the insulin chain) that runs as 17 kDa on deglycosylation (lanes 3 and 6).

mentioned above, photo-cross-linking of Pap^{B0} is markedly less efficient: relative to A8, B0-cross-linked complexes are reduced by >20-fold (lanes 4, 8, 12, and 16 in Figure 6). In each case, no covalent complex is observed in the absence of irradiation or in control studies of the Pmp^{B25} precursor.

To identify sites of cross-linking in the IR, we employed partial proteolysis with chymotrypsin to characterize fragments of the receptor α-subunit covalently bound to Pap-insulin derivatives (Figure 7). Digestions were undertaken under native conditions, so fragments reflect accessible chymotryptic sites within and between structural modules of the receptor; approximate sites of preferential chymotryptic cleavage are indicated in Figure 7C (arrows; see Experimental Procedures). An initial screen exploited the prior characterization of an N-terminal 47 kDa chymotryptic glycosylated fragment of the α-subunit by Pilch and colleagues (*49*) and the availability of antiserum to an N-terminal epitope (designated IR_{α}-N in the figures; Santa Cruz Biotechnology, Data Sheet sc-710). Upon deglycosylation, the apparent mass of this fragment on SDS−PAGE is 29−30 kDa, so it contains 245−260 amino acids. Analysis of limited chymotryptic digests demonstrates that Pap^{B16} contacts the N-terminal chymotryptic fragment (lanes 1−4 in panels A and B of Figure 7), in accord with its binding to the L1 β-helix domain (*47*). As expected, Pap^{B25} does not contact this N-terminal chymotryptic fragment but does contact a distinct 34 kDa fragment (lanes 5−8 in panels A and B of Figure 7), which therefore must contain the C-terminal region of the α-subunit derived from the insert domain (residues 704−718; *10*). Remarkably, Pap^{A8}, although predicted to contact the L1 domain (*11*), cross-links to the same fragment as the B25 derivative and not to the N-terminal fragment (lanes 9−12 in panels A and B of Figure 7). On further chymotryptic digestion, the 34 kDa fragment is cleaved to 20 kDa (lanes 2 and 5 in Figure 7D), which on deglycosylation yields a 17 kDa adduct (lanes 3 and 6 in Figure 7D). The digestion patterns of the A8 and B25 cross-linked complexes are essentially identical (lanes 2 and 3 vs

lanes 5 and 6 in Figure 7D, respectively), indicating that both A8 and B25 contact the same C-terminal 14 kDa domain of the α-subunit. Weak cross-linking by the Pap^{B0} derivative was not further characterized.

DISCUSSION

The IR is a receptor tyrosine kinase containing α- and *β*-subunits (Figure 1B). Encoded by a single gene, the α-subunit binds insulin whereas the transmembrane *β*-subunit contains a cytoplasmic kinase domain. Although the structure of the $\alpha_2\beta_2$ holoreceptor is not known, important insights have been obtained by sequence analysis and homology modeling (*27*, *58*). The α-subunit is a modular structure containing a series of distinct domains (L1, CR, L2, Fn0, and the N-terminal portion of Fn1/ID). Mutagenesis and domain "swap" studies suggest that the major insulin-binding regions are contained within the L1 *β*-helix domain, first fibronectin homology domain ($FnIII_0$), and C-terminal tail derived from the ID (*59*−*61*). Additional contacts with the central L2 domain and fibronectin homology regions have been suggested by cross-linking studies (*10*, *62*). Specific binding to insulin is observed to a 70 kDa monomeric minimized receptor containing the tripartite L1−CR−L2 motif (CR, cysteine-rich domain) and Fn0 tethered to a C-terminal tail derived from the ID (*61*). A structural model of the holoreceptor−insulin complex has been proposed at atomic resolution based on low-resolution EM image reconstruction and computer-based docking (*11*−*13*). Although specific contacts are predicted (see below), the resolution of the EM data (20 Å) and the uncertain assumptions employed in the docking algorithm preclude its utility at present in the design of novel analogues. These images nonetheless suggest that the insulin molecule is engulfed within the larger ectodomain of the IR.

The putative receptor-binding surface of insulin has been extensively investigated by mutagenesis and chemical modification (for review, see refs *2* and *27*). Structure−function relationships have been delineated by alanine scanning mutagenesis (*63*) and extended by chemical synthesis of selected analogues refractory to biosynthetic expression (*35*, *64*, *65*). These studies yield a general trend: alanine substitutions that significantly impair activity occur at conserved sites, whereas well-tolerated substitutions occur at nonconserved sites. This and related studies suggest that the conserved surface of insulin is engaged at a well-packed hormone−receptor interface. Stringent steric requirements at opposing surfaces are indicated by severe decreases in affinity incurred following subtle changes in side chain shape or volume, such as Ile^{A2} → Leu, Val^{A3} → Leu, Val^{B12} → Leu, and Phe^{B25} → Leu (decreased by 22-, 555-, 33-, and 50-fold, respectively; *31*, *64*); this surface is proposed to include side chains (such as A2 and A3; shaded region in Figure 1A) that are largely inaccessible in the native state of the hormone (*66*). Given the evolutionary optimization of such close packing, can the potency of insulin be enhanced by protein engineering?

Two "experiments of nature" led to characterization of substitutions that enhance the affinity of insulin for its receptor: Thr^{A8} → His and His^{B10} → Asp. His^{A8} was originally observed as a species variant among birds and fish (*18*−*22*, *25*). Although these divergent insulins contain multiple sequence differences, introduction of His^{A8} into human insulin augments its activity by 2−5-fold (*17*, *22*, *25*). Asp^{B10} was originally observed in a human pedigree in association with diabetes mellitus and hyperproinsulinemia (*67*). Although the mutation impairs the proper trafficking of the mutant proinsulin to the glucose-regulated secretory granule in the *β*-cell (*68*), the corresponding substitution in human insulin enhances binding to the receptor by 2-fold (*69*). Remarkably, each of these substitutions enhances the thermodynamic stability of insulin (*17*), seemingly via analogous mechanisms. The Thr^{A8} → His substitution in principle improves the α-helical propensity and C-Cap potential of the A1−A8 α-helix, whereas Asp^{B10} enhances the N-Cap potential of the B9−B19 α-helix. On the basis of these and related observations that certain low-affinity analogues exhibit reduced stability, Kaarsholm and colleagues proposed a correlation between stability and activity (*17*). These observations in turn suggested that thermodynamic optimization of the free hormone might provide a basis for designing analogues with enhanced activity (*17*). This possibility seemed to be attractive as the proposed strategy would circumvent the structural complexity of the receptor itself. Unfortunately, a recent study of multiple A8 analogues suggests that such a correlation is not generally observed and thus that explicit consideration of the IR will be necessary in understanding determinants of activity (*22*, *25*).

We envisage that the affinity of insulin may be enhanced by retaining the conserved framework of receptor contacts while optimizing nonconserved interactions at the edge of the hormone−receptor interface. This study was designed to test whether the enhanced activity of His^{A8}-insulin might reflect such a mechanism. Previous studies suggested that the A1−A8 α-helix functions as a preformed recognition element[10] (*54*, *55*). The diversity of side chains that are accommodated at A8 with little change in affinity suggests that this site, unlike conserved classical contacts at positions A2, A3, B12, B24, and B25, is not closely packed at the interface (*25*). In a pioneering model of a specific complex between insulin and the IR, Yip and colleagues interpreted EM images (*70*) to dock the T-state structure of insulin (crystallographic protomer 1BEN) within the interior of the ectodomain (*11*). In this model, Thr^{A8} and Tyr^{B16} are proposed to contact dimer-related L1 domains in the $\alpha_2\beta_2$ heterotetramer. The side chain of the Thr^{A8} is near Arg86 on the flat surface the L1 domain (predicted inter-side chain distance of 2.6 Å; *13*). The enhanced affinity of His^{A8}-insulin was ascribed to a stabilizing contact between its imidazole ring and the side chain Asp59 of the L1 domain (*11*). Such

[10] That the A1−A8 α-helix functions as a preformed recognition element is suggested by the study of a two-disulfide analogue in which internal cystine A6−A11 is pairwise substituted with either serine or alanine (*4*, *54*, *90*). The analogues are essentially identical in structure and stability: each exhibits segmental unfolding of the A1−A8 α-helix in an otherwise native-like subdomain. Restoration of this helix after receptor binding is implied by relative activities: the alanine analogue is 30-fold more active than the serine analogue, in quantitative accord with empirical tables of helical propensities and solvent transfer hydrophobic free energies (*54*). Substitution of Val^{A3} with Pap results in a low-affinity analogue (relative activity of 1%) that cross-links with high efficiency to the insulin receptor. Interpretation of this result in relation to native hormone−receptor recognition is unclear as CD spectra of the analogue indicate a decreased α-helix content and so possible perturbation of the A1−A8 α-helix, including the photoactive probe (unpublished results).

a charge-stabilized hydrogen bond between His^{A8} and the L1 β-helix would be reminiscent of the A4−A8 contact observed here in the T-state protomer of the crystallographic hexamer. The model also predicts that Tyr^{B16} contacts a similar region of the L1 domain (residue L87) in the other α-subunit (*11*).

Our study provides an experimental test of aspects of the Yip model. Although Tyr^{B16} indeed contacts the L1 domain (*47*), Pap^{A8} cross-links instead to a 14 kDa C-terminal domain derived from the FnI/ID region. Contacts with this domain are not visualized in the Yip model. Although the structure of the ID is enigmatic, a model of FnI has been proposed on the basis of crystal structures of the fibronectin (FN) type III domain (*71*−*73*). Such domains, ∼90 residues in length, consist of upper and lower antiparallel β-sheets (containing four and three β-strands, respectively). All seven strands are connected by loops of variable length (*72*). Whereas the Fn0 and Fn1 domains of the IR may be deleted in monomeric minimized receptor constructs, the ID-derived tail of the α-subunit (residues 704−719) is critical to receptor binding (*61*, *74*). Alanine scanning mutagenesis of the tail of the secreted ectodomain (residues 704−716) demonstrated that 10 of these 14 residues contributed to insulin binding; severe impairment (>1000-fold decreases in affinity) was observed following substitutions at four sites. It would be of future interest to determine if Pap^{A8} (like Pap^{B25}) contacts this critical region or instead introduces a novel contact peripheral to the major hormone-binding site in the ID. The diversity of amino acids that are functionally well tolerated at A8 (*25*) favors the latter possibility.

The discrepancy between these A8 cross-linking results and the Yip model (*11*) does not necessarily require a major reassessment of domain assignments in the EM image reconstruction (*12*) as a variety of types of evidence suggests three-dimensional contiguity between the N- and C-terminal domains of the α-subunit (*61*, *75*, *76*). Of particular interest are studies of a truncated high-affinity analogue (designated X92; *77*). This analogue lacks the five C-terminal residues of the B chain (B26−B30; *43*). Comparison of intact insulin and X92 enabled the role of the C-terminal segment of the B chain to be probed in the hormone−receptor complex (*77*). Two key substitutions in the IR were observed by Whittaker and colleagues to impair binding of insulin more significantly than binding of X92. Remarkably, one of the alanine substitutions is in the amino-terminal L1 domain (R14A), whereas the other is in the C-terminal tail derived from the ID (H710A). Control studies demonstrated that such differential binding was due to C-terminal truncation of the B chain and not to substitutions elsewhere in the protein (*77*). Whittaker and colleagues thus proposed that the N- and C-terminal domains of the receptor each contact the C-terminal region of the B chain, and hence must themselves be close together (*77*). It is therefore possible that only small adjustments in the EM-derived model might be necessary to accommodate our findings.

An intriguing hypothesis envisages that a single insulin molecule employs major and minor receptor-binding surfaces to bind two α-subunits simultaneously (*43*, *78*). Such an "internal dimer" would mimic the explicit hormone-induced dimerization of receptors for a number of hematopoietic hormone and cytokines (such as growth hormone, prolactin, and tumor necrosis factor; *79*−*83*). It is possible that the IR activation mechanism resembles the erythropoietin signaling system in which binding of a bivalent ligand to a preformed dimer leads to nonlocal structural rearrangement of the receptor with approximation of the two subunits (*84*). It is possible that insulin-induced changes in the relative orientation of α-subunits also reposition the β-subunits, leading to activation of their TK activity (*78*). In light of these hypotheses, it is possible that Pap^{A8} and Pap^{B25}, although each efficient in cross-linking to the C-terminal domain of the α-subunit, are in fact binding to different α-subunits.

CONCLUDING REMARKS

To our knowledge, this study provides the first explicit evidence that α-helices in both the A and B chains contact the IR. Mapping of A8 cross-linking to the C-terminal FnI/ID domain, although consistent with the critical importance of the ID-derived tail in hormone binding (*10*, *61*, *77*), is not in accord with a high-resolution model of the insulin−IR complex (*11*). This discrepancy may reflect the possibility that insulin docks in an orientation different from that proposed in the model (requiring global adjustment of the model), that the hormone undergoes a change in conformation on binding to the IR (confounding an assumption of the model), and/or that His^{A8} alters the overall mode of binding of insulin (relative to native human insulin). We favor the hypothesis that insulin undergoes a change in conformation on binding, so models based on docking of crystallographic protomers are likely to be misleading. In the future, such model building procedures could be refined on the basis of biochemical characterization of multiple Pap analogues with precise mapping of contact points by mass spectrometry. A definitive picture of the hormone−receptor complex awaits crystallographic analysis.

ACKNOWLEDGMENT

We thank D. F. Steiner for the P3-A cell line overexpressing the IR, G. D. Smith and C. C. Yip for the gift of the purified ectodomain, and G. G. Dodson, P. De Meyts, M. Snider, Q. X. Hua, M. Shoham, and V. Yee for helpful discussion.

SUPPORTING INFORMATION AVAILABLE

Zn-binding sites of the $T_3R_3^f$ coordination geometry model (Figure S1), the environment of the phenol molecule bound in the R_3^f trimer (Figure S2) and tables of rmsd values obtained for alignments of the crystal structure presented herein with other crystal structures. This material is available free of charge via the Internet at http://pubs.acs.org.

REFERENCES

1. Dodson, G., and Steiner, D. (1998) The role of assembly in insulin's biosynthesis, *Curr. Opin. Struct. Biol. 8*, 189−194.
2. Baker, E. N., Blundell, T. L., Cutfield, J. F., Cutfield, S. M., Dodson, E. J., Dodson, G. G., Hodgkin, D. M., Hubbard, R. E., Isaacs, N. W., and Reynolds, C. D. (1988) The structure of 2Zn pig insulin crystals at 1.5 Å resolution, *Philos. Trans. R. Soc. London 319*, 369−456.
3. Olsen, H. B., Ludvigsen, S., and Kaarsholm, N. C. (1996) Solution structure of an engineered insulin monomer at neutral pH, *Biochemistry 35*, 8836−8845.

4. Hua, Q. X., Hu, S. Q., Frank, B. H., Jia, W., Chu, Y. C., Wang, S. H., Burke, G. T., Katsoyannis, P. G., and Weiss, M. A. (1996) Mapping the functional surface of insulin by design: Structure and function of a novel A-chain analogue, *J. Mol. Biol. 264*, 390−403.
5. Brange, J., Ribel, U., Hansen, J. F., Dodson, G., Hansen, M. T., Havelund, S., Melberg, S. G., Norris, F., Norris, K., and Snel, L. (1988) Monomeric insulins obtained by protein engineering and their medical implications, *Nature 333*, 679−682.
6. Buse, J. B. (2001) Insulin analogues, *Curr. Opin. Endocrinol. Diabetes 8*, 95−100.
7. Yip, C. C., Hsu, H., Patel, R. G., Hawley, D. M., Maddux, B. A., and Goldfine, I. D. (1988) Localization of the insulin-binding site to the cysteine-rich region of the insulin receptor α-subunit, *Biochem. Biophys. Res. Commun. 157*, 321−329.
8. Wedekind, F., Baer-Pontzen, K., Bala-Mohan, S., Choli, D., Zahn, H., and Brandenburg, D. (1989) Hormone binding site of the insulin receptor: Analysis using photoaffinity-mediated avidin complexing, *Biol. Chem. 370*, 251−258.
9. Shoelson, S. E., Lee, J., Lynch, C. S., Backer, J. M., and Pilch, P. F. (1993) Bpa^{B25} insulins. Photoactivatable analogues that quantitatively cross-link, radiolabel, and activate the insulin receptor, *J. Biol. Chem. 268*, 4085−4091.
10. Kurose, T., Pashmforoush, M., Yoshimasa, Y., Carroll, R., Schwartz, G. P., Burke, G. T., Katsoyannis, P. G., and Steiner, D. F. (1994) Cross-linking of a B25 azidophenylalanine insulin derivative to the carboxyl-terminal region of the α-subunit of the insulin receptor. Identification of a new insulin-binding domain in the insulin receptor, *J. Biol. Chem. 269*, 29190−29197.
11. Yip, C. C., and Ottensmeyer, P. (2003) Three-dimensional structural interactions of insulin and its receptor, *J. Biol. Chem. 278*, 27329−27332.
12. Luo, R. Z., Beniac, D. R., Fernandes, A., Yip, C. C., and Ottensmeyer, F. P. (1999) Quaternary structure of the insulin−insulin receptor complex, *Science 285*, 1077−1080.
13. Ottensmeyer, F. P., Beniac, D. R., Luo, R. Z., and Yip, C. C. (2000) Mechanism of transmembrane signaling: Insulin binding and the insulin receptor, *Biochemistry 39*, 12103−12112.
14. Steiner, D. F., Chan, S. J., Welsh, J. M., and Kwok, S. C. (1985) Structure and evolution of the human insulin gene, *Annu. Rev. Genet. 19*, 463−484.
15. Brange, J., Hansen, J. F., Langkjaer, L., Markussen, J., Ribel, U., and Sorensen, A. R. (1992) Insulin analogues with improved absorption characteristics, *Horm. Metab. Res. Suppl. 26*, 125−130.
16. Marki, F., de Gasparo, M., Eisler, K., Kamber, B., Riniker, B., Rittel, W., Sieber, P., and Hoppe Seylers, Z. (1979) Synthesis and biological activity of seventeen analogues of human insulin, *Physiol. Chem. 360*, 1619−1632.
17. Kaarsholm, N. C., Norris, K., Jorgensen, R. J., Mikkelsen, J., Ludvigsen, S., Olsen, O. H., Sorensen, A. R., and Havelund, S. (1993) Engineering stability of the insulin monomer fold with application to structure−activity relationships, *Biochemistry 32*, 10773−10778.
18. Reid, K. M., Grant, P. T., and Youngson, A. (1968) A sequence of amino acids in insulin isolated from islet tissue of the cod (*Gadus callarias*), *J. Biochem. 110*, 289−296.
19. Weitzel, G., Oertel, W., Roger, K., and Kemmler, W. (1969) Insulin from the turkey (*Melegris gallopavo*), *Hoppe Seyler's Z. Physiol. Chem. 350*, 57−62.
20. Renner, R., and Kemmler, W. (1974) Mechanism of the increased biological activity of turkey insulin, *Hoppe Seyler's Z. Physiol. Chem. 355*, 1555−1556.
21. Conlon, J. M. (2001) Evolution of the insulin molecule: Insights into structure−activity and phylogenetic relationships, *Peptides 22*, 1183−1193.
22. Weiss, M. A., Hua, Q.-X., Jia, W., Nakagawa, S. H., Chu, Y.-C., Hu, S.-Q., and Katsoyannis, P. G. (2001) Activities of monomeric insulin analogs at position A8 are uncorrelated with their thermodynamic stabilities, *J. Biol. Chem. 276*, 40018−40024.
23. Mynarcik, D. C., and Whittaker, J. (1995) Insulin receptor transmembrane signaling: Evidence for an intermolecular oligomerization mechanism of action, *J. Recept. Signal Transduction Res. 15*, 887−904.
24. Simon, J., Freychet, P., Rosselin, G., and De Meyts, P. (1977) Enhanced binding affinity of chicken insulin in rat liver membranes and human lymphocytes: Relationship to the kinetic properties of hormone-receptor interaction, *Endocrinology 100*, 115−121.
25. Weiss, M. A., Wan, Z., Zhao, M., Chu, Y. C., Nakagawa, S. H., Burke, G. T., Jia, W., Hellmich, R., and Katsoyannis, P. G. (2002) Non-standard insulin design: Structure−activity relationships at the periphery of the insulin receptor, *J. Mol. Biol. 315*, 103−111.
26. Ciszak, E., and Smith, G. D. (1994) Crystallographic evidence for dual coordination around zinc in the T_3R_3 human insulin hexamer, *Biochemistry 33*, 1512−1517.
27. De Meyts, P., and Whittaker, J. (2002) Structural biology of insulin and IGF-I receptors: Implications for drug design, *Nat. Rev. Drug Discovery 1*, 769−783.
28. Pullen, R. A., Lindsay, D. G., Wood, S. P., Tickle, I. J., Blundell, T. L., Wollmer, A., Krail, G., Brandenburg, D., Zahn, H., Gliemann, J., and Gammeltoft, S. (1976) Receptor-binding region of insulin, *Nature 259*, 369−373.
29. De Meyts, P., Van Obberghen, E., and Roth, J. (1978) Mapping of the residues responsible for the negative cooperativity of the receptor-binding region of insulin, *Nature 273*, 504−509.
30. Weiss, M. A., Hua, Q. X., Lynch, C. S., Frank, B. H., and Shoelson, S. E. (1991) Heteronuclear 2D NMR studies of an engineered insulin monomer: Assignment and characterization of the receptor-binding surface by selective ^{2}H and ^{13}C labeling with application to protein design, *Biochemistry 30*, 7373−7389.
31. Shoelson, S. E., Lu, Z. X., Parlautan, L., Lynch, C. S., and Weiss, M. A. (1992) Mutations at the dimer, hexamer, and receptor-binding surfaces of insulin independently affect insulin−insulin and insulin−receptor interactions, *Biochemistry 31*, 1757−1767.
32. Brems, D. N., Alter, L. A., Beckage, M. J., Chance, R. E., DiMarchi, R. D., Green, L. K., Long, H. B., Pekar, A. H., Shields, J. E., and Frank, B. H. (1992) Altering the association properties of insulin by amino acid replacement, *Protein Eng. 5*, 527−533.
33. DiMarchi, R. D., Mayer, J. P., Fan, L., Brems, D. N., Frank, B. H., Green, J. K., Hoffman, J. A., Howey, D. C., Long, H. B., Shaw, W. N., Shields, J. E., Slieker, L. J., Su, K. S. E., Sundell, K. L., and Chance, R. E. (1992) in *Peptides: Proceedings of the Twelfth American Peptide Symposium* (Smith, J. A., and Rivier, J. E., Eds.) pp 26−28, ESCOM Science Publishers B.V., Leiden, The Netherlands.
34. Merrifield, R. B., Vizioli, L. D., and Boman, H. G. (1982) Synthesis of the antibacterial peptide cecropin A (1−33), *Biochemistry 21*, 5020−5031.
35. Hu, S. Q., Burke, G. T., Schwartz, G. P., Ferderigos, N., Ross, J. B., and Katsoyannis, P. G. (1993) Steric requirements at position B12 for high biological activity in insulin, *Biochemistry 32*, 2631−2635.
36. Chu, Y. C., Hu, S. Q., Zong, L., Burke, G. T., Gammeltoft, S., Chan, S., Steiner, D. F., and Katsoyannis, P. G. (1994) Insulin-like compounds related to the amphioxus insulin-like peptide, *Biochemistry 33*, 11278−11285.
37. Wan, Z., Xu, B., Chu, Y. C., Katsoyannis, P. G., and Weiss, M. A. (2003) Crystal structure of *allo*-Ile^{A2}-insulin, an inactive chiral analogue: Implications for the mechanism of receptor binding, *Biochemistry 42*, 12770−12783.
38. Brunger, A. T., Adams, P. D., Clore, G. M., DeLano, W. L., Gros, P., Grosse-Kunstleve, R. W., Jiang, J. S., Kuszewski, J., Nilges, M., Pannu, N. S., Read, R. J., Rice, L. M., Simonson, T., and Warren, G. L. (1998) Crystallography & NMR system: A new software suite for macromolecular structure determination, *Acta Crystallogr. D54*, 905−921.
39. Jones, T. A., Zou, J. Y., Cowan, S. W., and Kjeldgaard, M. (1991) Improved methods for binding protein models in electron density maps and the location of errors in these models, *Acta Crystallogr. A47*, 110−119.
40. Laskowski, R. A., Macarthur, M. W., Moss, D. S., and Thornton, J. M. (1993) PROCHECK: A program to check the stereochemical quality of protein structures, *J. Appl. Crystallogr. 26*, 283−291.
41. Brunger, A. T. (1993) *XPLOR Manual, Version 3.1*, Yale University Press, New Haven, CT.
42. Yoshimasa, Y., Paul, J. I., Whittaker, J., and Steiner, D. F. (1990) Effects of amino acid replacements within the tetrabasic cleavage site on the processing of the human insulin receptor precursor expressed in Chinese hamster ovary cells, *J. Biol. Chem. 265*, 17230−17237.
43. Schäffer, L. (1994) A model for insulin binding to the insulin receptor, *Eur. J. Biochem. 221*, 1127−1132.
44. Paul, J. I., Tavare, J., Denton, R. M., and Steiner, D. F. (1990) Baculovirus-directed expression of the human insulin receptor and an insulin-binding ectodomain, *J. Biol. Chem. 265*, 13074−13083.

45. Cara, J. F., Mirmira, R. G., Nakagawa, S. H., and Tager, H. S. (1990) An insulin-like growth factor I/insulin hybrid exhibiting high potency for interaction with the type I insulin-like growth factor and insulin receptors of placental plasma membranes, *J. Biol. Chem. 265*, 17820−17825.
46. Xu, B., Hu, S. Q., Chu, Y. C., Nakagawa, S. H., Whittaker, J., Katsoyannis, P. G., and Weiss, M. A. (2004) Diabetes-associated mutations in insulin: Consecutive residues in the B chain contact distinct domains of the insulin receptor, *Biochemistry 43*, 8356−8372.
47. Huang, K., Xu, B., Hu, S. Q., Chu, Y. C., Hua, Q. X., Qu, Y., Li, B., Wang, S., Wang, R. Y., Nakagawa, S. H., Theede, A. M., Whittaker, J., De Meyts, P., Katsoyannis, P. G., and Weiss, M. A. (2004) How insulin binds: the β-chain alpha-helix contacts the L1 beta-helix of the insulin receptor, *J. Mol. Biol. 341*, 529−550.
48. Boni-Schnetzler, M., Scott, W., Waugh, S. M., DiBella, E., and Pilch, P. F. (1987) The insulin receptor. Structural basis for high affinity ligand binding, *J. Biol. Chem. 262*, 8395−8401.
49. Waugh, S. M., DiBella, E. E., and Pilch, P. F. (1989) Isolation of a proteolytically derived domain of the insulin receptor containing the major site of cross-linking/binding, *Biochemistry 28*, 3448−3455.
50. Herzberg, V. L., Grigorescu, F., Edge, A. S., Spiro, R. G., and Kahn, C. R. (1985) Characterization of insulin receptor carbohydrate by comparison of chemical and enzymatic deglycosylation, *Biochem. Biophys. Res. Commun. 129*, 789−796.
51. Garrett, T. P., McKern, N. M., Lou, M., Frenkel, M. J., Bentley, J. D., Lovrecz, G. O., Elleman, T. C., Cosgrove, L. J., and Ward, C. W. (1998) Crystal structure of the first three domains of the type-1 insulin-like growth factor receptor, *Nature 394*, 395−399.
52. Bentley, G., Dodson, E., Dodson, G., Hodgkin, D., and Mercola, D. (1976) Structure of insulin in 4-zinc insulin, *Nature 261*, 166−168.
53. Whittingham, J. L., Chaudhuri, S., Dodson, E. J., Moody, P. C., and Dodson, G. G. (1995) X-ray crystallographic studies on hexameric insulins in the presence of helix-stabilizing agents, thiocyanate, methylparaben, and phenol, *Biochemistry 34*, 15553−15563.
54. Weiss, M. A., Hua, Q.-X., Jia, W., Chu, Y.-C., Wang, R.-Y., and Katsoyannis, P. G. (2000) Hierarchiacal protein "un-design": Insulin's intrachain disulfide bridge tethers a recognition α-helix, *Biochemistry 39*, 15429−15440.
55. Olsen, H. B., Ludvigsen, S., and Kaarsholm, N. C. (1998) The relationship between insulin bioactivity and structure in the NH_2-terminal A-chain helix, *J. Mol. Biol. 284*, 477−488.
56. Eberle, A. N., and de Graan, P. N. E. (1985) General principles for photoaffinity labeling of peptide hormone receptors, *Methods Enzymol. 109*, 129−157.
57. Weiss, M. A., Nakagawa, S. H., Jia, W., Xu, B., Hua, Q. X., Chu, Y. C., Wang, R. Y., and Katsoyannis, P. G. (2002) Protein structure and the spandrels of San Marco: Insulin's receptor-binding surface is buttressed by an invariant leucine essential for protein stability, *Biochemistry 41*, 809−819.
58. Peitsch, M. C., Herzyk, P., Wells, T. N., and Hubbard, R. E. (1996) Automated modelling of the transmembrane region of G-protein coupled receptor by Swiss-model, *Recept. Channels 4*, 161−164.
59. Williams, P. F., Mynarcik, D. C., Yu, G. Q., and Whittaker, J. (1995) Mapping of an NH_2-terminal ligand binding site of the insulin receptor by alanine scanning mutagenesis, *J. Biol. Chem. 270*, 3012−3016.
60. Mynarcik, D. C., Yu, G. Q., and Whittaker, J. (1996) Alanine-scanning mutagenesis of a C-terminal ligand binding domain of the insulin receptor α subunit, *J. Biol. Chem. 271*, 2439−2442.
61. Kristensen, C., Wiberg, F. C., Schaffer, L., and Andersen, A. S. (1998) Expression and characterization of a 70-kDa fragment of the insulin receptor that binds insulin. Minimizing ligand binding domain of the insulin receptor, *J. Biol. Chem. 273*, 17780−17786.
62. Fabry, M., Schaefer, E., Ellis, L., Kojro, E., Fahrenholz, F., and Brandenburg, D. (1992) Detection of a new hormone contact site within the insulin receptor ectodomain by the use of a novel photoreactive insulin, *J. Biol. Chem. 267*, 8950−8956.
63. Kristensen, C., Kjeldsen, T., Wiberg, F. C., Schaffer, L., Hach, M., Havelund, S., Bass, J., Steiner, D. F., and Andersen, A. S. (1997) Alanine scanning mutagenesis of insulin, *J. Biol. Chem. 272*, 12978−12983.
64. Nakagawa, S. H., and Tager, H. S. (1992) Importance of aliphatic side-chain structure at positions 2 and 3 of the insulin A chain in insulin-receptor interactions, *Biochemistry 31*, 3204−3214.
65. Weiss, M. A., Hua, Q. X., Jia, W., Nakagawa, S. H., Chu, Y. C., and Katsoyannis, P. G. (2002) in *Insulin & Related Proteins: Structure to Function and Pharmacology* (Dieken, M. L., Federwisch, M., and De Meyts, P., Eds.) pp 103−119, Kluwar Academic Publishers, Dordrecht, The Netherlands.
66. Xu, B., Hua, Q. X., Nakagawa, S. H., Jia, W., Chu, Y. C., Katsoyannis, P. G., and Weiss, M. A. (2002) Chiral mutagensis of insulin's hidden receptor-binding surface: Structure of an *allo*-isoleucine A2 analogue, *J. Mol. Biol. 316*, 435−441.
67. Chan, S. J., Seino, S., Gruppuso, P. A., Schwartz, R., and Steiner, D. F. (1987) A mutation in the B chain coding region is associated with impaired proinsulin conversion in a family with hyperproinsulinemia, *Proc. Natl. Acad. Sci. U.S.A. 84*, 2194−2197.
68. Steiner, D. F., and Chan, S. J. (1988) An overview of insulin evolution, *Horm. Metab. Res. 20*, 443−444.
69. Schwartz, G. P., Burke, G. T., and Katsoyannis, P. G. (1987) A superactive insulin: [B10-aspartic acid]insulin(human), *Proc. Natl. Acad. Sci. U.S.A. 84*, 6408−6411.
70. Luo, Y., and Baldwin, R. L. (1999) The 28−111 disulfide bond constrains the α-lactalbumin molten globule and weakens its cooperativity of folding, *Proc. Natl. Acad. Sci. U.S.A. 96*, 11283−11287.
71. O'Bryan, J. P., Frye, R. A., Cogswell, P. C., Neubauer, A., Kitch, B., Prokop, C., Espinosa, R. r., Le Beau, M. M., Earp, H. S., and Liu, E. T. (1991) axl, a transforming gene isolated from primary human myeloid leukemia cells, encodes a novel receptor tyrosine kinase, *Mol. Cell. Biol. 11*, 5016−5031.
72. Potts, J. R., and Campbell, I. D. (1996) Structure and function of fibronectin modules, *Matrix Biol. 15*, 313−320.
73. Marino-Buslje, C., Martin-Martinez, M., Mizuguchi, K., Siddle, K., and Blundell, T. L. (1999) The insulin receptor: From protein sequence to structure, *Biochem. Soc. Trans. 27*, 715−726.
74. Kristensen, C., Andersen, A. S., Ostergaard, S., Hansen, P. H., and Brandt, J. (2002) Functional reconstitution of insulin receptor binding site from non-binding receptor fragments, *J. Biol. Chem. 277*, 18340−18345.
75. Brandt, J., Andersen, A. S., and Kristensen, C. (2001) Dimeric fragment of the insulin receptor α-subunit binds insulin with full holoreceptor affinity, *J. Biol. Chem. 276*, 12378−12384.
76. Surinya, K. H., Molina, L., Soos, M. A., Brandt, J., Kristensen, C., and Siddle, K. (2002) Role of insulin receptor dimerization domains in ligand binding, cooperativity, and modulation by anti-receptor antibodies, *J. Biol. Chem. 277*, 16718−16725.
77. Mynarcik, D. C., Williams, P. F., Schäffer, L., Yu, G. Q., and Whittaker, J. (1997) Analog binding properties of insulin receptor mutants. Identification of amino acids interacting with the COOH terminus of the B-chain of the insulin molecule, *J. Biol. Chem. 272*, 2077−2081.
78. De Meyts, P. (1994) The structural basis of insulin and insulin-like growth factor-I receptor binding and negative co-operativity, and its relevance to mitogenic versus metabolic signalling, *Diabetologia 37* (Suppl. 2), S135−S148.
79. Livnah, O., Stura, E. A., Middleton, S. A., Johnson, D. L., Jolliffe, L. K., and Wilson, I. A. (1999) Crystallographic evidence for preformed dimers of erythropoietin receptor before ligand activation, *Science 283*, 987−990.
80. Goffin, V., and Kelly, P. A. (1997) The prolactin/growth hormone receptor family: Structure/function relationships, *J. Mammary Gland Biol. Neoplasia 2*, 7−17.
81. Postel-Vinay, M. C., and Kelly, P. A. (1996) Growth hormone receptor signalling, *Bailliere's Clin. Endocrinol. Metab. 10*, 323−336.
82. Castellino, A. M., and Chao, M. V. (1996) Trans-signaling by cytokine and growth factor receptors, *Cytokine Growth Factor Rev. 7*, 297−302.
83. Banner, D. W., D'Arcy, A., Janes, W., Gentz, R., Schoenfeld, H. J., Broger, C., Loetscher, H., and Lesslauer, W. (1993) Crystal structure of the soluble human 55 kd TNF receptor-human TNFβ complex: Implications for TNF receptor activation, *Cell 73*, 431−435.
84. Syed, R. S., Reid, S. W., Li, C., Cheetham, J. C., Aoki, K. H., Liu, B., Zhan, H., Osslund, T. D., Chirino, A. J., Zhang, J., Finer-Moore, J., Elliott, S., Sitney, K., Katz, B. A., Matthews, D. J., Wendoloski, J. J., Egrie, J., and Stroud, R. M. (1998) Efficiency of signalling through cytokine receptors depends critically on receptor orientation, *Nature 395*, 511−516.
85. Pierce, S. B., Costa, M., Wisotzkey, R., Devadhar, S., Homburger, S. A., Buchman, A. R., Ferguson, K. C., Heller, J., Platt, D. M.,

Pasquinelli, A. A., Liu, L. X., Doberstein, S. K., and Ruvkun, G. (2001) Regulation of DAF-2 receptor signaling by human insulin and ins-1, a member of the unusually large and diverse *C. elegans* insulin gene family, *Genes Dev. 15*, 672−686.

86. Blundell, T. L., Cutfield, J. F., Cutfield, S. M., Dodson, E. J., Dodson, G. G., Hodgkin, D. C., Mercola, D. A., and Vijayan, M. (1971) Atomic positions in rhombohedral 2-zinc insulin crystals, *Nature 231*, 506−511.
87. Derewenda, U., Derewenda, Z., Dodson, E. J., Dodson, G. G., Reynolds, C. D., Smith, G. D., Sparks, C., and Swenson, D. (1989) Phenol stabilizes more helix in a new symmetrical zinc insulin hexamer, *Nature 338*, 594−596.
88. Badger, J., Harris, M. R., Reynolds, C. D., Evans, A. C., Dodson, E. J., Dodson, G. G., and North, A. C. (1991) Structure of the pig insulin dimer in the cubic crystal, *Acta Crystallogr. B47*, 127−136.
89. Chothia, C., Lesk, A. M., Dodson, G. G., and Hodgkin, D. C. (1983) Transmission of conformational change in insulin, *Nature 302*, 500−505.
90. Dai, Y., and Tang, J. G. (1996) Characteristic, activity and conformational studies of [A6-Ser, A11-Ser]-insulin, *Biochim. Biophys. Acta 1296*, 63−68.

BI048223F